Control of Airborne Aromatic Hydrocarbons over TiO$_2$-Carbon Nanotube Composites

Joon Y. Lee, Seung H. Shin, Ho H. Chun, Wan K. Jo

Abstract—Poly vinyl acetate (PVA)-based titania (TiO$_2$)–carbon nanotube composite nanofibers (PVA-TCCNs) with various PVA-to-solvent ratios and PVA-based TiO$_2$ composite nanofibers (PVA-TN) were synthesized using an electrospinning process, followed by thermal treatment. The photocatalytic activities of these nanofibers in the degradation of airborne monocyclic aromatics under visible-light irradiation were examined. This study focuses on the application of these photocatalysts to the degradation of the target compounds at sub-part-per-million indoor air concentrations. The characteristics of the photocatalysts were examined using scanning electron microscopy, X-ray diffraction, ultraviolet-visible spectroscopy, and Fourier-transform infrared spectroscopy. For all the target compounds, the PVA-TCCNs showed photocatalytic degradation efficiencies superior to those of the reference PVA-TN. Specifically, the average photocatalytic degradation efficiencies for benzene, toluene, ethyl benzene, and o-xylene (BTEX) obtained using the PVA-TCCNs with a PVA-to-solvent ratio of 0.3 (PVA-TCCN-0.3) were 11%, 59%, 89%, and 92%, respectively, whereas those observed using PVA-TNs were 5%, 9%, 28%, and 32%, respectively. PVA-TCCN-0.3 displayed the highest photocatalytic degradation efficiency for BTEX, suggesting the presence of an optimal PVA-to-solvent ratio for the synthesis of PVA-TCCNs. The average photocatalytic efficiencies for BTEX decreased from 11% to 4%, 59% to 18%, 89% to 37%, and 92% to 53%, respectively, when the flow rate was increased from 1.0 to 4.0 L min^{-1}. In addition, the average photocatalytic efficiencies for BTEX increased 11% to ~0%, 59% to 3%, 89% to 7%, and 92% to 13%, respectively, when the input concentration increased from 0.1 to 1.0 ppm. The prepared PVA-TCCNs were effective for the purification of airborne aromatics at indoor concentration levels, particularly when the operating conditions were optimized.

Keywords—Mixing ratio, nanofiber, polymer, reference photocatalyst.

I. INTRODUCTION

PERSONAL exposure to airborne aromatics is of significant concern, because of the wide distribution of these pollutants in both indoors and outdoors, and their adverse health effects. Monocyclic aromatic hydrocarbons such as benzene, toluene, ethyl benzene, and xylene (BTEX), in particular, are frequently reported at high concentrations in atmospheric environments [1]. Atmospheric aromatics are mainly emitted from road traffic, industrial and residential combustion of fossil fuels, and industrial use of petroleum and petrochemical products [2], [3]. Indoor aromatics originate from the penetration of atmospheric aromatics as well as a range of indoor sources [2], [4]. These aromatic compounds have been closely linked to various adverse health effects, e.g., sick building syndrome, central nervous system and kidney damage, and leukemia and other types of cancer [5].

Recently, advanced oxidation photocatalysis using semiconducting TiO$_2$ has become one of the most attractive techniques for solving environmental problems, because of its high photochemical reactivity, photocorrosion resistance, and chemical stability [6]-[9]. Nevertheless, TiO$_2$ has certain weaknesses in practical applications for pollutant purification, especially its wide band gap, i.e., > 3.2 eV, low adsorption capacity, and low quantum yield as a result of rapid recombination of photo-induced charge carriers [10]. These shortcomings can be tackled by coupling TiO$_2$ with carbon nanotubes (CNTs) to prepare TiO$_2$–CNT composites [11]. CNTs have a high adsorption capacity for environmental contaminants; therefore, the photocatalytic performance of TiO$_2$ can be improved by combination with CNTs [12], [13]. CNTs can also act as a photosensitizing agent that allows visible-light absorption, which makes TiO$_2$–CNT composites functional under visible-light exposure [14]. Moreover, photo-induced electrons in the space–charge segregation region at the CNT/TiO$_2$ interface can be moved into the CNTs, resulting in holes on the TiO$_2$, and this reduces the recombination rates of electron and holes [11]. Previous studies [15], [16] have shown that the photocatalytic activities under visible-light irradiation of TiO$_2$–CNT composites are superior to those of stand-alone TiO$_2$ in the decomposition of a range of environmental contaminants; this was attributed to their enhanced adsorption and electronic properties.

Recently, [17], [18] have coupled TiO$_2$ with polymers to prepare polymer-supported TiO$_2$ nanofibers, using an electrospinning process. They demonstrated that the prepared photocatalysts can be used effectively for the photocatalytic degradation of methylene blue and rhodamine B in the aqueous phase, without any post-separation problems. Polymers have a distinct advantage over other supporting substrates, namely the larger surface area of the nanofibrous mat structure [19]. Moreover, a synergistic effect between polymer supporting materials and TiO$_2$–CNT composites in the photocatalytic degradation of environmental pollutants has been suggested. Hu et al. [20] and Kedem et al. [21] used polymer-based TiO$_2$–CNT composite nanofibers for the photocatalytic degradation of methyl orange and rhodamine 6G in aqueous

J. Y. Lee and S. H. Shin are with the department of environmental engineering, Kyungpook National University, Daegu, 702–701, Korea (e-mail: jlee2@knu.ac.kr, ssho@knu.ac.kr).

H. H. Chun is with the department of Naval Architecture and Ocean Engineering, Pusan National University, Busan 609-735, Korea (e-mail: chunahh@pusan.ac.kr).

W. K. Jo is with the the department of environmental engineering, Kyungpook National University, Daegu, 702–701, Korea (corresponding author to provide phone: +82-53-950-6584; fax: +82-53-950-6584; e-mail: wkjo@ knu.ac.kr).

World Academy of Science, Engineering and Technology
International Journal of Environmental and Ecological Engineering
Vol:9, No:2, 2015

media, respectively, and showed that their photocatalytic performances were better than those of pure TiO_2 and TiO_2–CNT composites. The photocatalytic activities of polymer-based TiO_2–CNT composite nanofibers for environmental applications may depend on their polymer-to-solvent mixing ratios, which can change the morphological characteristics of the composite nanofibers, e.g., the fiber diameter and bead structure. Pilehrood et al. [22] reported that the morphological characteristics of polyacrylonitrile (PAN)-based TiO_2–CNT composite nanofibers varied with the mixing ratio of the polymer to N,N-dimethylformamide (DMF), which was used as a solvent. However, the effects of polymer-to-solvent ratios on the photocatalytic activities of polymer-based TiO_2–CNT composite nanofibers have not been fully explored. Moreover, previous researchers used ultraviolet (UV) lamps as the photocatalytic light source, but these nanofibers may also be active under visible light, because of the role of CNTs as a potential photosensitizing agent [14].

In the current study, poly vinyl acetate (PVA)-based TiO_2–CNT composite nanofibers (PVA-TCCNs) with different PVA-to-solvent ratios were synthesized using an electrospinning method and thermal post treatment. In addition, the photocatalytic activities of the PVA-TCCNs in the degradation of airborne monocycle aromatics (BTEX) were examined under visible-light irradiation. This study focuses on the use of the synthesized photocatalysts for the degradation of BTEX at sub-part-per-million (ppm) indoor air concentrations, rather than hundreds-ppm concentrations, which are more closely associated with industrial emission levels. PVA was selected as the base polymer because it is cheap and hydrophobic [23]. The photocatalytic activity of a PVA-supported TiO_2 nanofiber (PVA-TN) was also investigated for comparison with that of a representative PVA-TCCN.

II. EXPERIMENTAL METHODS

A. Photocatalytic Synthesis

PVA-TCCNs with four different PVA-to-solvent mixing ratios, i.e., 0.1, 0.2, 0.3, and 0.4, which were denoted by PVA-TCCN-0.1, PVA-TCCN-0.2, PVA-TCCN-0.3, and PVA-TCCN-0.4, respectively, were synthesized using an electrospinning process, followed by thermal treatment. Multi-walled CNT (MWNT)–COOH was prepared by treating MWNTs (Carbon Nano Technology Co., Korea) with concentrated HNO_3 solution (Sigma Aldrich) in a reflux apparatus. MWNTs (1 g) were added to HNO_3 solution (60 mL). The mixture was sonicated for 1 h, refluxed at 115 °C for 18 h, and then concentrated using a rotary evaporator (HS Science HS-2005S). The concentrated product was cleaned using deionized water and dried at 60 °C for 30 h under vacuum conditions.

The prepared MWNT–COOH was coupled with a Ti source and PVA to synthesize PVA-TCCNs with different PVA-to-solvent ratios. MWNT–COOH (0.005 g) was mixed with acetic acid (5 mL) and then, sonicated for 1 h (Solution A). Titanium isopropoxide (6.2 mL, TIP; Sigma Aldrich) was mixed with acetic acid and stirred for 2 h (Solution B), and PVA (1.0, 2.0, 3.0, or 4.0 g) was mixed with N,N-dimethyl formamide (10 mL, DMF; Sigma Aldrich) and stirred for 2 h (Solution C). Four different PVA weights were utsed to synthesize PVA-TCCN-0.1, PVA-TCCN-0.2, PVA-TCCN-0.3, and PVA-TCCN-0.4. Solution B was added to Solution C and the mixture was stirred vigorously with Teflon-coated magnetic bars to prepare Solution D; this solution was mixed with Solution A under sonication to synthesize the final PVA-TCCN solution. A PVA-TN solution with a PVA-to-solvent ratio of 0.3 (denoted by PVA-TN) was also prepared using the same procedure, but without mixing with MWNT–COOH solution. Each final solution was transferred to a stainless-steel-spinneret plastic syringe. A piece of clean aluminum foil was placed 15 cm below the spinneret and a DC voltage of 20 kV was supplied. The electrospun nanofibers were dried at 80°C for 12 h under vacuum conditions and calcined at 500°C for 1 h. The prepared PVA-TCCNs and PVA-TN were characterized using scanning electron microscopy (SEM; Hitachi S-4300 & EDX-350 FE-SEM), X-ray diffraction (XRD; Rigaku D-max 2500), UV-visible spectroscopy (Varian CARY 5G spectrophotometer), and Fourier-transform infrared (FTIR; PerkinElmer Spectrum GX spectrophotometer) spectroscopy.

B. Determination of Photocatalytic Activity

The photocatalytic performances of the photocatalysts in the degradation of airborne aromatics were investigated using an annular-type Pyrex reactor. The inside-wall of the reactor was coated with one of the PVA-TCCNs or PVA-TN. A cylindrical visible-light lamp (F8T5DL, Youngwha Lamp Co.) was placed inside the annular tube, and acted as the inner wall of the Pyrex tube. Zero-grade dry air was delivered by a compressed air cylinder, and purified by passing through an activated carbon filter. This dry air was flowed through a humidification device. The humidified air was then directed to a mixing chamber, where the liquid-phase standard compounds (BTEX) were mixed. This airstream was then moved to the annular Pyrex reactor. The BTEX concentrations were adjusted to specified values by mixing the humidified air with the target compounds. The relative humidity (RH) was controlled to 50%, and was measured at the reactor inlet. The flow rate (FR) was adjusted to 1.0 L min^{-1} using mass flow meters. When the humidity level at the reactor outlet port reached a steady state, the photocatalytic system was pre-purified for 3 h by passing clean humidified air through it. After the absence of BTEX contamination of the experimental system was confirmed, the BTEX mixture was transferred to the system. For the adsorption tests, BTEX samples were collected, in the absence of light, at the upstream and downstream sites of the reactor. After the adsorption tests, the lamp was activated to determine the photocatalytic activities of the prepared photocatalysts.

The BTEX photocatalytic degradation efficiencies of of the photocatalysts were examined under several specified operating conditions, based on the FRs and input concentrations (ICs). The FRs used in this study were 1.0, 2.0, 3.0, and 4.0 L min^{-1}, to cover a wide FR range, and the ICs were

World Academy of Science, Engineering and Technology
International Journal of Environmental and Ecological Engineering
Vol:9, No:2, 2015

0.1, 0.5, 0.7, and 1.0 ppm, which were within indoor air concentrations [4]. The RH was fixed at 50%, which is within the comfort levels for building residents. For the evaluation of FR effects, the IC was adjusted to 0.1 ppm, and for the evaluation of IC effects, the FR was fixed at 1.0 L min^{-1}. The distance from the inside wall of the Pyrex tube to the outside wall of the lamp was 1.0 cm. The weight of the photocatalyst coating was approximately 3.3 mg cm^{-2}.

Airstream sampling was performed by filling an empty Teflon bag every hour at both the inlet and outlet of the reactor. The air samples were transferred to a Tenax TA sorbent trap. All sampling was performed at ambient temperature (19−24°C). BTEX adsorbed on the Tenax TA was analyzed using a gas chromatograph (Perkin Elmer Clarus 680)/mass spectrometer (Perkin Elmer Clarus SQ8 T) coupled with an automated thermal desorber (Perkin Elmer ATD 350). The peaks of compounds other than the target chemical species on the gas chromatograms were not high enough to be quantified. For this analytical procedure, quality control was performed by analyzing laboratory blank and spiked trap samples. On each experimental day, one laboratory blank sample was analyzed to observe any contamination of trap samples. In addition, one standard sample was analyzed to observe daily change in instrumental responses. When any change in the responses deviated from that calculated from a specified calibration curve by more than 10%, another calibration curve was prepared. The method detection limits ranged from 0.6 to 1.1 ppb, depending on the chemical species.

III. RESULTS AND DISCUSSION

A. Characteristics of PVA-TCCNs and PVA-TN

Fig. 1 shows the morphological characteristics of the four PVA-TCCNs with different ratios of PVA-to-solvent (PVA-TCCN-0.1, PVA-TCCN-0.2, PVA-TCCN-0.3, and PVA-TCCN-0.4) and PVA-TN. The PVA-TCCNs had fibrous structures, although some of them were broken into rods, confirming that composite nanofibers could be prepared using a combination of electrospinning and thermal post-treatment. These results were attributed to penetration of solvent molecules into the long chains of polymer substrates, thereby reducing or eliminating agglomeration of solvent molecules [24]. It is worth noting that PVA-TCCN-0.1, which was prepared using the lowest PVA-to-solvent ratio, had a strong tendency to form beads as well as fibers. The formation of beads by PVA-TCCN-0.1 was ascribed to the surface tension caused by excess solvent molecules, which leads to agglomeration [24]. Pilehrood et al. [22] observed beads or spindles in PAN-based TiO$_2$–MWNT composite nanofibers synthesized using an electrospinning process under low PAN-to-solvent (DMF) conditions, but they observed smooth fibers under high PAN-to-solvent conditions. Aryal et al. [23] successfully synthesized PVA-based TiO$_2$–CNT composite nanofibers with a fixed PVA-to-solvent (DMF) ratio, using a sol-gel process followed by electrospinning. Our results, obtained using Image Tool software (Version 3.00, University of Texas Health Science Center, San Antonio, TX, USA),

showed that the thickness of the PVA-TCCNs increased with increasing PVA-to-solvent (DMF) ratio: the average thicknesses were 0.06, 0.25, 0.31, and 0.36 μm for PVA-TCCN-0.1, PVA-TCCN-0.2, PVA-TCCN-0.3, and PVA-TCCN-0.4, respectively. The differences were ascribed to interactions between PVA and the TiO$_2$ photocatalyst. In addition, PVA-TCCN-0.3 had the smoothest fibers, with the lowest number of broken structures, indicating that there is an optimal PVA-to-solvent ratio.
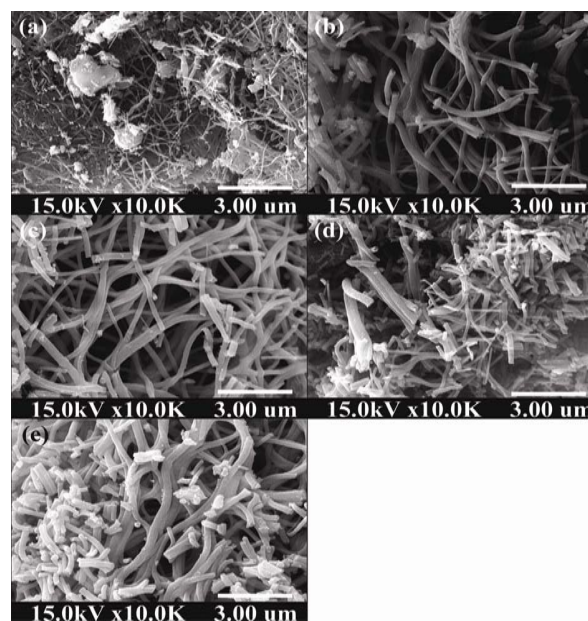

Fig. 1 Scanning electron microscopy of four PVA-TCCNs with different ratios of PVA to solvent: (a), PVA-TCCN-0.1; (b), PVA-TCCN-0.2; (c), PVA-TCCN-0.3; (d), PVA-TCCN-0.4; and (e) PVA-TN

Fig. 2 shows the XRD patterns for the four PVA-TCCNs and PVA-TN. The photocatalysts calcined at 500°C for 1 h showed crystalline phases, whereas the uncalcined one was amorphous (data not shown). The PVA-TCCNs and PVA-TN showed several anatase forms, including a major peak at $2\theta = 25.2^{\circ}$, but did not display any distinctive rutile crystal forms. These results indicate that the thermal post-treatment is essential when PVA-TCCNs are prepared using electrospinning. Aryal et al. [23] also observed only anatase crystal forms in the XRD patterns of non-woven mats of TiO$_2$–CNT composites prepared using TIP as the Ti source and calcined at 400 and 500 °C for 2 h. In contrast, several studies have shown that the XRD pattern of Degussa P25 TiO$_2$ particles exhibits several anatase forms, including a major peak at $2\theta = 25.2^{\circ}$, and several rutile forms, including a major peak at $2\theta = 27.4^{\circ}$ [25]-[27]

Fig. 3 shows the UV-visible spectra of the four PVA-TCCNs and PVA-TN. The PVA-TCCNs displayed shifting of the visible absorption edges relative to that of Degussa P25 TiO$_2$ (around 420 nm), as reported in [28]. The light-absorption intensities of the PVA-TCCNs were also higher than that of PVA-TN. As mentioned previously, these results were ascribed to the role of CNTs as potential photosensitizing agents in the

World Academy of Science, Engineering and Technology
International Journal of Environmental and Ecological Engineering
Vol:9, No:2, 2015

PVA-TCCNs [14]. Moreover, the absorption intensity of the visible-range edge of the PVA-TCCNs increased as the PVA-to-solvent ratio increased. This was attributed to the greater thickness of the PVA-TCCNs at high polymer concentrations. These findings therefore demonstrate that the prepared PVA-TCCNs can act as effective photocatalysts under visible-light irradiation.
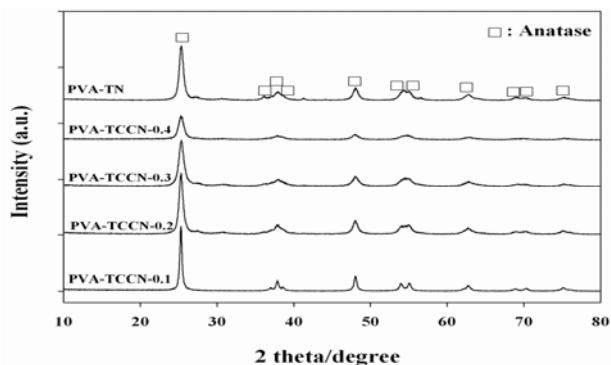
Fig. 2 X-ray diffraction patterns of four PVA-TCCNs with different ratios of PVA to solvent (PVA-TCCN-0.1, PVA-TCCN-0.2, PVA-TCCN-0.3, and PVA-TCCN-0.4) and PVA-TN
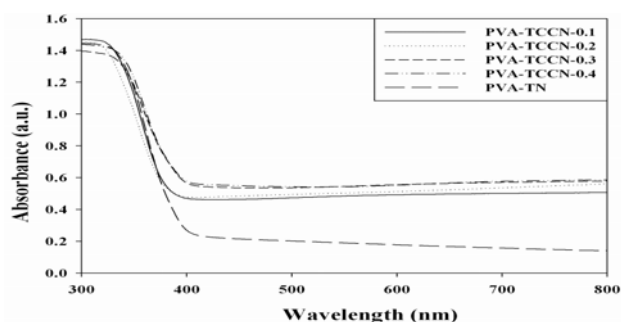

Fig. 3 UV-visible spectra of four PVA-TCCNs with different ratios of PVA to solvent (PVA-TCCN-0.1, PVA-TCCN-0.2, PVA-TCCN-0.3, and PVA-TCCN-0.4) and PVA-TN
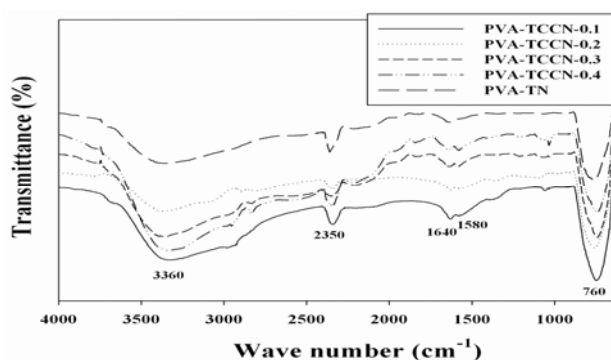

Fig. 4 Fourier transform infrared of four PVA-TCCNs with different ratios of PVA to solvent (PVA-TCCN-0.1, PVA-TCCN-0.2, PVA-TCCN-0.3, and PVA-TCCN-0.4) and PVA-TN

Fig. 4 shows the FTIR spectra of the four PVA-TCCNs and PVA-TN. PVA-TN showed four major bands, at 3360, 2350, 1640, and 760 cm^{-1}, and the PVA-TCCNs displayed these four bands and one additional band, at 1580 cm^{-1}. The broad band at

3360 cm^{-1} was ascribed to the stretching vibration of hydroxyl groups on the photocatalyst surface. The intensities of this band for the PVA-TCCNs was stronger than that for PVA-TN, suggesting that there are larger amounts of hydroxyl groups in the PVA-TCCNs. The band observed at 2350 cm^{-1} was ascribed to asymmetric stretching of CO_2 gas present in the laboratory [29]. The band at 1640 cm^{-1} was related to the bending of hydroxyl groups derived from water molecules adsorbed on the photocatalysts surfaces [28]. For the photocatalysts, the broad band at 760 cm^{-1} was associated with a combination of stretching and bending of Ti–O and O–Ti–O [23]. The band at 1580 cm^{-1} was only observed for the PVA-TCCNs, and was attributed to CNTs, indicating that CNTs were successfully impregnated into the TiO_2 nanofibers. The band for PVA-TN at 760 cm^{-1} was shifted to slightly lower wavelength for the PVA-TCCNs; this was attributed to strong interactions between TiO_2 and the CNTs [20].

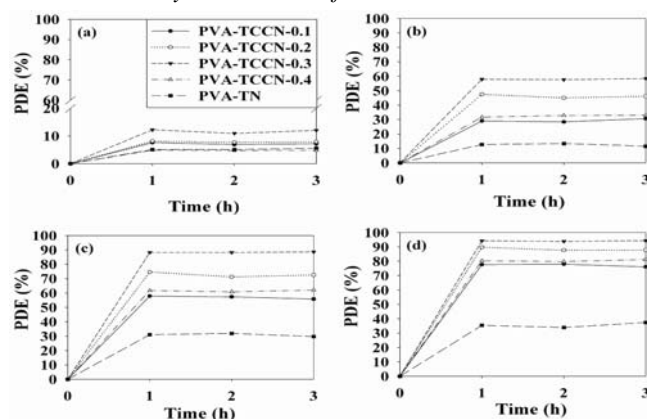### B. Photocatalytic Activities of PVA-TCCNs and PVA-TN

Fig. 5 Time-dependent photocatalytic decomposition efficiencies of (a) benzene, (b) toluene, (c) ethyl benzene, and (d) o-xylene as determined via four PVA-TCCNs with different ratios of PVA to solvent (PVA-TCCN-0.1, PVA-TCCN-0.2, PVA-TCCN-0.3, and PVA-TCCN-0.4) and PVA-TN under visible-light irradiation

The photocatalytic activities of PVA-TCCNs with various PVA-to-solvent ratios and PVA-TN in the degradation of BTEX under visible-light exposure were investigated. Fig. 5 exhibits the time-dependent photocatalytic degradation efficiencies for BTEX over PVA-TCCN-0.1, PVA-TCCN-0.2, PVA-TCCN-0.3, PVA-TCCN-0.4, and PVA-TN. In all cases, the photocatalytic degradation efficiencies of the PVA-TCCNs were higher than those achieved with PVA-TN. For example, the time-series average degradation efficiencies for BTEX using PVA-TCCN-0.3 were 11%, 59%, 89%, and 92%, respectively, whereas those obtained using PVA-TN were 5%, 9%, 28%, and 32%. In addition, PVA-TCCN-0.3 showed the highest efficiency among the prepared PVA-TCCNs, indicating that there is an optimal PVA-to-solvent ratio for the preparation of PVA-TCCNs. These results were supported by the UV-visible spectra, in which the PVA-TCCN-0.3 showed the smoothest fibers with the fewest broken structures. This is consistent with the results reported by [21], who found that the photocatalytic activities of PAN-based TCCNs in the

World Academy of Science, Engineering and Technology
International Journal of Environmental and Ecological Engineering
Vol:9, No:2, 2015

degradation of an aqueous dye (rhodamine B) were higher than that obtained using a PAN-based TiO_2 photocatalyst. The enhanced photocatalytic function of the PVA-TCCNs was probably the results of the synergistic properties of three materials (PVA, TiO_2, and MWCNT) in the photocatalytic degradation of BTEX. PVA-based TCCNs can therefore be used efficiently for the photocatalytic degradation of gaseous toxic chemicals under visible-light exposure.

The degradation efficiencies of PVA-TCCN-0.3 for BTEX under visible-light exposure at various FRs are shown in Fig. 6. The efficiency decreased with increasing FR; this was consistent with the results obtained by other researchers, who used pure TiO_2 or other types of photocatalyst [30], [31]. Specifically, the average photocatalytic efficiencies of BTEX decreased from 11% to 4%, 59% to 18%, 89% to 37%, and 92% to 53%, respectively, when the FR was increased from 1.0 to 4.0 L min^{-1}. These findings indicate that the FR is an important parameter in the mechanism of degradation by PVA-TCCNs. When the FR is increased, the bulk mass transport of chemical species from the airstream to the photocatalyst surface increases, probably by convection and diffusion. The photocatalytic degradation rate could therefore increase when the FR is increased, indicating that the photocatalytic degradation of BTEX is limited to the photocatalyst surface. However, the air retaining time in the reactor under higher FR conditions would not be enough to achieve complete transfer of the BTEX molecules from the airstream to the photocatalyst surface. The air retaining times were 7.5, 3.8, 2.5, and 1.8 s for FRs of 1.0, 2.0, 3.0, and 4.0 L min^{-1}, respectively. These times were estimated by dividing the photocatalytic reactor volume by the matched value of each FR. The lower degradation efficiencies under high FR conditions indicate that the effect of a short reaction time might exceed the mass transfer effect in the photocatalytic degradation of BTEX molecules.
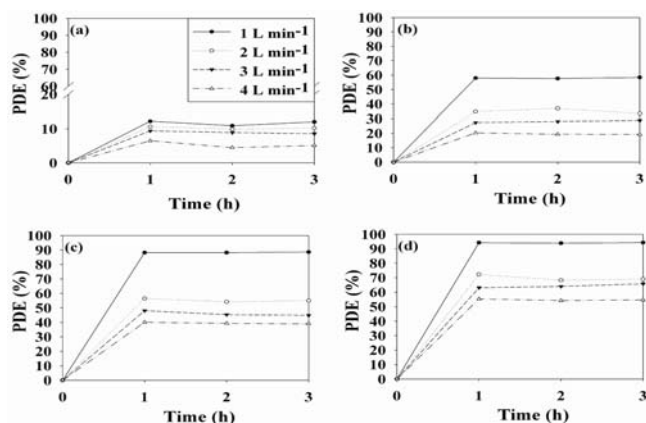

Fig. 6 Time- dependent photocatalytic decomposition efficiencies of (a) benzene, (b) toluene, (c) ethyl benzene, and (d) o-xylene as determined via PVA-TCCN-0.3 according to air flow rates.

Fig. 7 exhibits the BTEX degradation efficiencies of PVA-TCCN-0.3 at various ICs. The BTEX degradation efficiencies decreased with increasing IC; specifically, the average photocatalytic efficiencies for BTEX increased 11% to

~0%, 59% to 3%, 89% to 7%, and 92% to 13%, respectively, when the IC was increased from 0.1 to 1.0 ppm. These results indicate that the target compounds were degraded on the photocatalyst surface via first-order reaction kinetics. Jo [32] reported that the degradation efficiencies for monocyclic aromatic compounds by UV/ TiO_2–CNT units decreased, as the IC increased from 0.1 to 1.0 ppm. It is therefore suggested that, similar to those of pure TiO_2 photocatalysts, the activities of PVA-TCCNs in the degradation of BTEX can be changed within certain indoor air concentration ranges. The active adsorption sites on catalyst surfaces are important for the photocatalytic degradation of chemical species, therefore the dependence of photocatalytic degradation on IC observed in the present study was attributed to competition for adsorption sites among contaminant molecules on the photocatalyst surface.
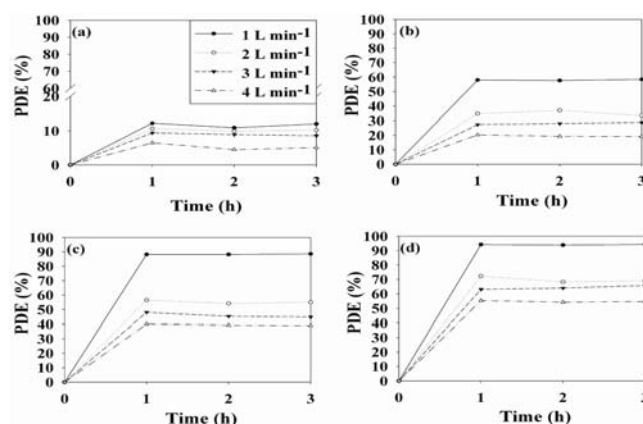

Fig. 7 Time- dependent photocatalytic decomposition efficiencies of (a) benzene, (b) toluene, (c) ethyl benzene, and (d) o-xylene as determined via PVA-TCCN-0.3 according to initial concentrations

IV. CONCLUSIONS

In this study, PVA-TCCNs with various PVA-to-solvent ratios and PVA-TN were prepared, and their photocatalytic activities under visible-light irradiation in the degradation of airborne BTEX at indoor concentration levels were determined. The morphological and spectroscopic characteristics of the prepared photocatalysts were examined. The SEM images showed that the prepared PVA-TCCNs had fibrous structures, although some of them were broken into rods, confirming that composite nanofibers could be prepared using a combination of electrospinning and thermal post-treatment. The UV-visible spectra showed that the PVA-TCCNs functioned effectively under visible-light irradiation. The photocatalytic degradation efficiencies of the PVA-TCCNs, for all the target compounds, were superior to those of a reference PVA-TN. It was shown that there is an optimal PVA-to-solvent ratio for the synthesis of PVA-TCCNs. In addition, the photocatalytic activities of the PVA-TCCNs in the photocatalytic degradation for BTEX depended on two operating parameters, i.e., FR and IC. Taken together, the results suggest that the prepared PVA-TCCNs could be effectively used for the purification of airborne aromatics at indoor concentration levels.

World Academy of Science, Engineering and Technology
International Journal of Environmental and Ecological Engineering
Vol:9, No:2, 2015

REFERENCES

[1] M. de Blas, M. Navazo, L. Alonso, N. Durana, M. Gomez, and C, Iza J. Sci Total Environ, 2012, 426: 327.
[2] M. Masiol, C. Agostinelli, G. Formenton, E. Tarabotti, and B. Pavoni, Sci Total Environ, 2014, 494-495: 84.
[3] M. C. McCarthy, Y. –A. Aklilu, S. G. Brown, and D. A. Lyder, Atmos Environ, 2013, 81: 504.
[4] F. –C. Su, B. Mukherjee, and S. Batterman, Environ Res, 2013, 126: 192.
[5] USEPA (United States of Environmental Agency), Health Effects Information Used In Cancer and Noncancer Risk Characterization for the 1999 National-Scale Assessment. Accessed in December 2012. http://www.epa.gov/ttn/atw/nata1999/99pdfs/healtheffectsinfo.pdf.
[6] W. Xie, H. Chen, X. Zhang, X. Hu, and G. Li, Chin J Catal, 2013, 34: 1076.
[7] Y. Zheng, Z. Pan, and X. Wang, Chin J Catal, 2013, 34: 524.
[8] L. G. Devi and R. Kavitha, Appl Catal B, 2013, 140-141: 559.
[9] K. Nakata and A. Fujishima, J Photochem Photobiol C, 2012, 13: 169.
[10] M. A. Henderson, Surf Sci Rep, 2011, 66: 185.
[11] R. Leary and A. Westwood, Carbon, 2011, 49: 741.
[12] S. M. Miranda, G. E. Romanos, V. Likodimos, R. R. N. Marques, E. P. Favvas, F. K. Katsaros, K. L. Stefanopoulos, V. J. P. Vilar, J. L. Faria, P. Falaras, and A. M. T. Silva, Appl Catal B, 2014, 147: 65.
[13] Z. Meng Z and W. Ou, Chin J Catal, 2012, 33: 1495.
[14] M. J. Sampaio, R. R. N. Marques, P. B. Tavares, J. L. Faria, A. M. T. Silva, and C. G. Silva, J Environ Chem Eng, 2013, 1: 945.
[15] M. Y. Guo, F. Liu, Y. H. Leung, A. M. C. Ng, A. B. Djurišić, and W. K. Chan, Curr Appl Phys, 2013, 13: 1280.
[16] K. Rajasekar, S. Thennarasu, R. Rajesh, R. Abirami, K. B. Ameen, A. Ramasubbu, Solid State Sci 2013, 26: 45.
[17] S. An, M. W. Lee, B. N. Joshi, A. Jo, Y. Jung, and S. S. Yoon, Ceramics Int, 2014, 40: 3305.
[18] L. Szatmáry, J. Šubrt, V. Kalousek, J. Mosinger, and K. Lang, Catal Today, 2014, 230: 74.
[19] C. Prahsarn, W. Klinsukhon, and N. Roungpaisan, Mater Lett, 2011, 65: 2498.
[20] G. Hu, X. Meng, X. Feng, Y. Ding, S. Zhang, and M. Yang, J Mater Sci, 2007, 42: 7162.
[21] S. Kedem, D.Rozen, Y. Cohen, and Y. Paz, J Phys Chem C, 2009, 113: 14893.
[22] M. K. Pilehrood, P. Heikkilä, and A. Harlin, Autex Res J, 2012, 12: 1
[23] S. Aryl, C. K. Kim, K. –W. Kim, M. S. Khil, and H. Y. Kim, Mater Sci Eng C, 2008, 28: 75.
[24] S. Singh, H. Mahalingam, and P. K. Singh, Appl Catal B, 2013, 462-463: 178.
[25] N. T. Nolan, D. W. Synnott, M. K. Seery, S. J. Hinder, A. Van Wassenhoven, and S. C. Pillai, J Hazard Mater, 2012, 211−212: 88.
[26] J. Li, S. L. Zhou, G. –B. Hong, and C. –T. Chang, Chem Eng J, 2013, 219: 486.
[27] A. Rey, P. García-Muñoz, M. D. Hernández-Alonso, E. Mena, S. García-Rodríguez, and F. J. Beltrán, Appl Catal B, 154-155: 274.
[28] W. K. Jo and H. J. Kang, Power Technol, 2013, 250: 115.
[29] J. C. S. Wu and Y. –T. Cheng, J Catal, 2006, 237: 393.
[30] W. Zhou, G. Du, P. Hu, Y. Yin, J. Li, J. Yu, G. Wang, J. Wang, H. Liu, J. Wang, and H. Zhang, J. Hazard. Mater., 2011, 197: 19.
[31] Z. Wang, J. Liu, Y. Dai, W. Dong, S. Zhang, and J. Chen, J Hazard Mater, 2012, 215−216: 25.
[32] W. K. Jo, J Air Waste Manage, 2013, 63: 963.

J. Y. Lee is a Ph. D student at the department of environmental engineering, Kyungpook National University, Korea.

H. H. Chun is the full professor at the department of Naval Architecture and Ocean Engineering, Pusan National University, Korea.

W. K. Jo is the full professor at the the department of environmental engineering, Kyungpook National University, Korea.